*Journal of Sound and Vibration* (2001) **246**(2), 349–373
doi:10.1006/jsvi.2001.3651, available online at http://www.idealibrary.com on IDEAL®

# INVESTIGATION OF THE AXIAL STIFFNESS OF A BOLT USING A THREE-DIMENSIONAL FINITE ELEMENT MODEL

R. I. ZADOKS

*Caterpillar Inc., Lafayette, IN* 47905, *U.S.A.*

AND

D. P. R. KOKATAM

*Altair Engineering Inc., Troy, MI* 48084, *U.S.A.*

(*Received* 9 *August* 1999, *and in final form* 26 *February* 2001)

The axial stiffness of a bolt plays a critical role in the prediction of the self-loosening process of threaded connections subject to oscillatory excitation. Since self-loosening is one of the most frequent failure modes for threaded connections, it is important to understand the mechanisms of this behavior. In this paper a three-dimensional finite element model of a single bolt threaded into a plate is used to determine values for the axial stiffness of the bolt. The model is loaded by pulling the nodes around the outside of the bolt head in the axial direction while holding the bottom of the plate fixed. Several analyses are performed to investigate the axial stiffness of the bolt. Quasistatic analysis predicts a linear relationship between the reaction force and the axial stretch of the bolt, indicating that the axial stiffness is constant. Dynamic analyses yield similar results if the prescribed accelerations are limited, though the predicted stiffness values are lower than those from the quasistatic analyses. Different dynamic loading patterns also yield slightly different stiffness values. Investigations from this research can be used to better predict the self-loosening process.



## 1. INTRODUCTION

Self-loosening, which is the reduction of clamping force due to any effect other than a direct torque on a bolt head or nut, is one of the most prominent causes of failure of threaded connections in mechanical assemblies. Even though considerable research has explored the self-loosening behavior of bolts, the exact mechanisms of this behavior had remained obscure until recent papers by Zadoks and Yu [1] and Hess [2] accurately predicted the self-loosening behavior of a single bolt subject to harmonic base excitations in the transverse and axial directions, respectively (see Figure 1).

Zadoks and Yu [1] analyzed the conditions needed for transversely loaded connections to loosen and stated that the off-torque in the bolt must overcome all of the frictional resistances for the bolt to loosen. With their experiments on a connection with a single bolt, as shown in Figure 1, they proved that impact is a sufficient condition for the bolt to loosen dynamically. They also modelled the threaded connection of their experiments as a two-degree-of-freedom mass–spring model, including the effects of bending and Hertz contact. With this analytical model these authors were able to accurately predict the

0022-460X/01/370349 + 25 $35.00/0 

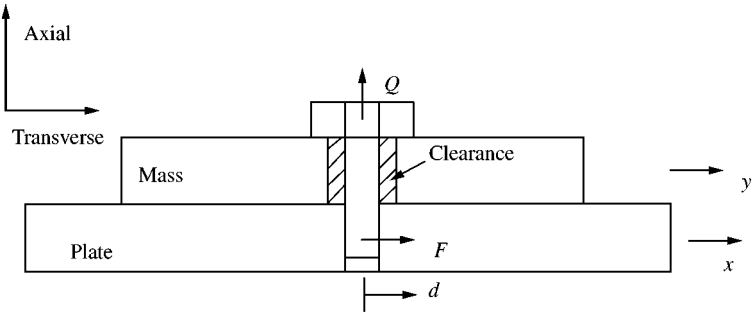


Figure 1. Schematic of the single bolted joint (after Zadoks and Yu [1]).

self-loosening process. However, some of the parameter values in the analytical model had to be adjusted to achieve these results. Axial stiffness, which determines the change in the bolt preload based on the rotation of the bolt, was one of the critical parameters that had to be adjusted in the prediction of the self-loosening process.

The adjustment of some of the parameter values in reference [1] serves as the motivation behind the current investigation of the axial stiffness of bolts. A powerful and sophisticated tool for understanding the behavior of mechanical systems is the finite element method (FEM). To determine the value of the axial stiffness of a bolt and, thereby, to better understand the self-loosening process, a three-dimensional finite element model of a threaded connection [3] is analyzed using the PRONTO3D and JAS3D FEM computer programs. PRONTO3D [4] is a finite element program for the analysis of the three-dimensional response of systems subjected to transient dynamic loading conditions. JAS3D [5] is a multi-strategy iterative code for quasistatic solid mechanics analysis. In a quasistatic analysis the inertial forces are assumed to be negligible when compared to the external (applied) forces and the internal (strain) forces, leading to a Newton's First Law of Motion formulation:

$$\sum \vec{F} = \vec{0}. \tag{1}$$

However, motion is still allowed, meaning that velocity and forces based on velocity are still included in the analysis.

## 2. FINITE ELEMENT MODEL DESCRIPTION

Zadoks and Kokatam [3] described the development of two different three-dimensional finite element models of a threaded connection like the one shown in Figure 1. These models were essentially identical in geometry, but differed in the refinement of certain portions of the mesh. The complex geometries of both the external and internal threads were realistically modelled, with different levels of fidelity in the two meshes. The more accurate model was referred to as the refined mesh, while the model with significant reductions in node and element counts was referred to as the coarse mesh. The coarse mesh has been used to perform all of the dynamic analyses and one of the two quasistatic analyses described in this paper. The goal of these analyses is to determine a value for the axial stiffness of the bolt, where axial stiffness is defined as the slope of the axial load versus axial stretch line. The selection of the appropriate axial stretch is discussed below.

TABLE 1

*Dimensions of the finite element model (after Zadoks and Kokatam [3])*

| Description | (mm) | (in) |
|---|---|---|
| Diameter of the bolt | 6·3500 | 0·25 |
| Width across flats of the bolt head | 10·9728 | 0·432 |
| Thickness of the bolt head | 4·2333 | 0·16667 |
| Length of the unthreaded shank | 14·8167 | 0·58333 |
| Length of the threaded shank | 16·9333 | 0·66667 |
| Outer radius of the plate | 28·3972 | 1·118 |
| Thickness of the plate | 12·7000 | 0·50 |

TABLE 2

*Material properties*

| Description | Value |
|---|---|
| Mass density (kg/m$^3$) | 7844· |
| Young's modulus (GPa) | 206·8 |
| The Poisson ratio | 0·292 |
| Proof strength (MPa) | 586·1 |
| Yield strength (0·2% offset) (MPa) | 634·3 |
| Ultimate strength (MPa) | 827·4 |
| Static friction coefficient | 0·20 |
| Kinematic friction coefficient | 0·20 |

The general threaded connection model of Figure 1 consists of a mass clamped to a plate by a bolt threaded into the plate. However, the clamped mass is not used in the current analyses to determine the axial stiffness of the bolt as the mass does not affect this value, and its exclusion reduces the computational costs. Model dimensions are shown in Table 1. The material properties used in the analyses are listed in Table 2. The friction coefficient values shown in Table 2 are for steel to steel dry contact and match the values used in reference [1].

The coarse mesh from reference [3] is shown in Figure 2, and a cross-sectional view of this mesh after zooming at the threaded region is presented in Figure 3. This mesh includes 38 500 nodes and 30 966 solid hexahedral elements. All of the nodes on the outside surface of the bolt head, along its thickness, are grouped as a node set (node set 1) and all of the nodes on the bottom surface of the plate are grouped as another node set (node set 2) for the application of boundary conditions during the analyses.

The most critical features of this model are the contacts between the meshes of the threads and other pieces of the model. Contact between surfaces is modelled in FEM codes with the help of a contact algorithm. The contact algorithm determines when contact is to be enforced and applies the resulting forces, as defined by physics, between the two contacting surfaces. Since the physics of contact is not fully understood, FEM contact algorithms generally allow the user to select from a variety of contact models, such as fixed (no relative motion between contacting surfaces), sliding without friction, and sliding with friction. Generally, contact algorithms require the user to define one of the contact surfaces as the master surface (usually the coarser mesh) and the other as the slave surface (usually the finer

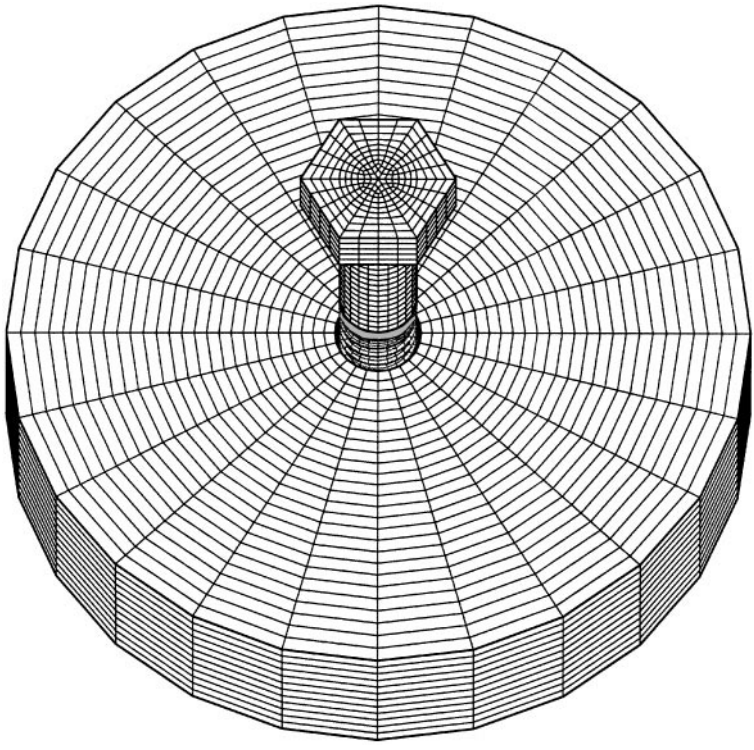

Figure 2. Finite element mesh of the bolt–plate system (after Zadoks and Kokatam [3]).

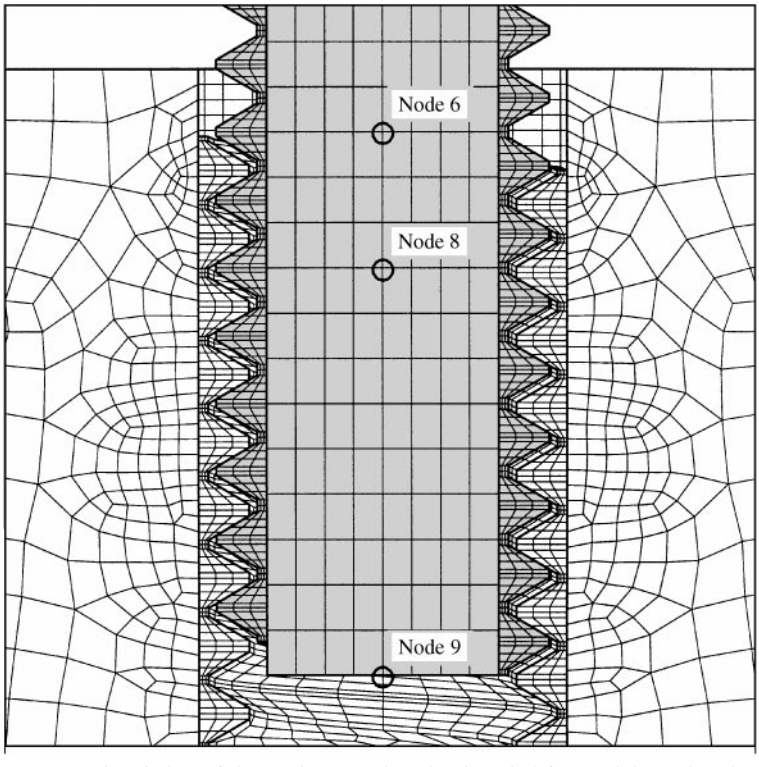


Figure 3. Cross-sectional view of the mesh zoomed at the threads (after Zadoks and Kokatam [3]).

mesh). This master–slave definition allows the contact algorithm to determine the movement of the slave nodes with respect to the master surface. Newer contact algorithms, like the one used in PRONTO3D [4], allow for the definition of a symmetric or balanced contact, where the two surfaces are treated as equals. While PRONTO3D allows the user to define a balanced contact pair, JAS3D is limited to master–slave contact relations [5].

Due to the helical nature of the thread forms and the need for smaller elements to get accurate results in these regions of the model, it would be very difficult and costly to define a mesh where nodes could be combined between component parts, such as the external threads and the rest of the bolt body. Therefore, the threads are meshed separately from the bolt and plate. However, the threads need to be modelled as being physically integral to their respective parts. This is accomplished in the FEM input by defining fixed contact between the inside and top surfaces of the external thread mesh and the bolt shank, and between the outside surface of the internal thread mesh and the plate. Note that the thread forms are both taken to be the slave surfaces in a master–slave contact relationship. Sliding friction is defined between the external and internal thread meshes. A Coulomb friction model is used in this contact algorithm, and the friction coefficient values used in the analyses described below are listed in Table 2. In the JAS3D quasistatic analyses the internal thread mesh is selected to be the master surface, while a balanced contact definition is employed at this interface in the PRONTO3D dynamic analyses [4, 5].

As stated previously, results from both quasistatic and dynamic FEM analyses are presented below. There are two major reasons for the inclusion of both types of analysis in this study. First, this work is meant to serve as a preliminary step in the development of a fully dynamic FEM simulation of the self-loosening process studied in reference [1]. Therefore, the dynamic results are included to show that PRONTO3D can produce accurate results for the model developed in reference [3]. Second, the quasistatic results are included to show that JAS3D can also produce accurate results for this model and to provide confirmation of the results predicted by PRONTO3D. It should be noted that the focus of the work reported here was on the viability of the dynamic analysis, and that the quasistatic results were generated almost exclusively for confirmation purposes.

## 3. DESCRIPTIONS OF THE LOADING CASES

To determine the axial stiffness of the bolt, the most realistic loading case would be to hold the plate fixed while applying a known force to the bolt head. This type of loading is difficult to apply in a physical system, as it is difficult to control the force being applied and to assure that the force is evenly distributed over the bolt head. A second approach, which is also used in tensile test machines, is to apply a known displacement to the bolt head while holding the plate fixed. The required force is then measured using a load cell. The difficulty in applying a realistic force distribution to the FEM model leads to the use of this latter loading condition.

To apply this loading condition to the FEM model, node set 2 is held fixed by applying "no displacement" boundary conditions in all three Cartesian directions, while node set 1 is subjected to a kinematic boundary condition in the axial ($z$) direction. For the quasistatic analyses a linearly varying displacement, starting at zero, with a slope equal to 36·83 mm/s is prescribed (see Figure 4). This slope was selected so that the ending displacement of the quasistatic analysis would nearly match the ending displacement from the dynamic Case 1 (b) analysis (8·103 μm versus 8·128 μm).

For the dynamic analyses the axial velocity is prescribed, leading to the displacement functions shown in Figure 4 (note that Case 1(a) is not shown for scaling purposes).

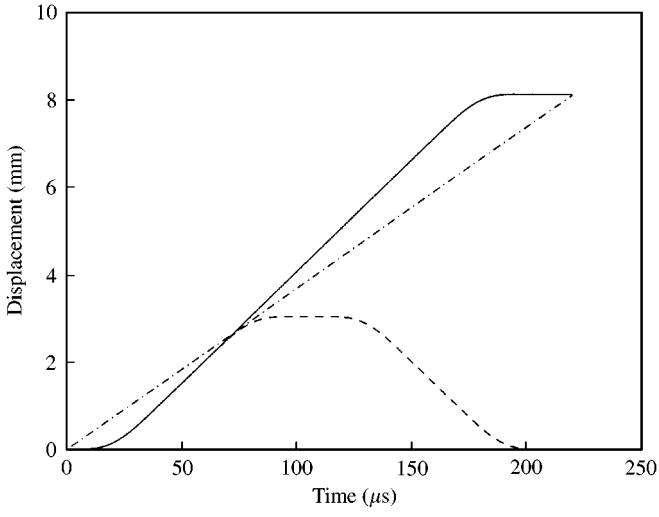


Figure 4. Time histories of the displacements applied to the bolt head: ——, dynamic Case 1(b); – – – – –, dynamic Case 2; —·—·—, quasistatic case.

A velocity boundary condition is applied because PRONTO3D does not allow for the direct application of a prescribed displacement [4]. Three different velocity functions are prescribed for the dynamic analyses. For Cases 1(a) and 1(b), the velocity starts at zero, increases cycloidally to a constant velocity value at 40 μs (which is 406·4 mm/s for Case 1(a) and 50·8 mm/s for Case 1(b)), decreases cycloidally from the constant value back to zero in the time range from 160 to 200 μs, and remains at zero until the end of the simulation at 220 μs. The cycloidal increasing and decreasing functions are respectively:

$$\bar{v}_{increase}(t) = \frac{\hat{t}}{\Delta t} - \frac{1}{2\pi}\sin\left(\frac{2\pi\hat{t}}{\Delta t}\right), \quad \bar{v}_{decrease}(t) = 1 - \frac{\hat{t}}{\Delta t} + \frac{1}{2\pi}\sin\left(\frac{2\pi\hat{t}}{\Delta t}\right), \tag{2, 3}$$

where $\Delta t$ is the time span of the cycloidal curve (40 μs in these examples) and $\hat{t}$ is an adjusted time that is equal to zero at the beginning of the cycloidal curve and equal to $\Delta t$ at the end of the curve. The velocity $v(t)$ is found by multiplying $\bar{v}(t)$ by a scale factor, which is 406·4 mm/s for Case 1(a) and 50·8 mm/s for Case 1(b).

For the third dynamic analysis (Case 2) the velocity function is identical to the function for Case 1(b) up to 60 μs. At 60 μs the Case 2 velocity function decreases cycloidally from the constant value back to zero at 100 μs, stays constant at zero until 110 μs, decreases cycloidally to the negative of the constant velocity value ( − 50·8 mm/s) at 150 μs, remains constant at this value until 170 μs, increase cycloidally back to zero at 210 μs, and remains constant at zero until the end of the simulation at 220 μs. The resulting displacement function for this loading case is shown in Figure 4.

The velocity scale factor for Case 1(a) was selected because it led to an axial force that was approximately equal to the design preload for this bolt. The design preload, which was selected to be 90 per cent of the proof load for the bolt, was calculated to be 10·82 kN for a standard, grade 5, 1/4 in diameter bolt with coarse threads [6]. The final axial force from the Case 1(a) simulation was found to be 10·88 kN. The velocity scale for Case 1(b) was selected to match the scale used in Case 2. The velocity scale for Case 2 was selected so that the maximum axial force would be approximately 534 N, which is twice the preload used in reference [1]. The maximum axial force from the Case 2 simulation was found to be 510·5 N.

Before presenting the results of the analyses, the loading patterns described above and shown in Figure 4 should be discussed. First, it should be noted that the time span for the loading is quite short (220 μs). This time was a compromise between a shorter time that was desired to reduce the computational time required by the FEM program, which is directly proportional to the number of time steps in the analysis, and a longer time that was desired to more accurately reflect a realistic load case and to reduce the dynamic effects in the FEM results. Essentially, the time selected was the smallest value that would yield reasonably clean dynamic simulation results with the Case 2 loading pattern.

For the dynamic simulations the time step is determined so that a stress wave takes more than one time step to cross any single element in the mesh. This is required for stability of the central difference integration algorithm implemented in PRONTO3D [4]. Since the entire mesh is composed of a single elastic material type (i.e., low carbon steel as indicated by the property values in Table 2), the stress wave speed is a constant given by

$$c = \sqrt{\frac{E(1-\mu)}{\rho(1+\mu)(1-2\mu)}} = 5894\,\text{m/s}, \tag{4}$$

where $E$ is Young's modulus, $\mu$ is the Poisson ratio, and $\rho$ is the mass density. The maximum stable time step is then found by dividing the smallest distance across an element by the value from equation (4). This time step value was found to be 0·00626 μs. Therefore, assuming that the time step remains constant there would be over 35 000 steps in a 220 μs simulation.

The dynamic effects that needed to be avoided were associated with the time for the reflection of a stress wave to return to its point of origin. Since the excitation was applied parallel to the bolt's axis, the wave reflection time was determined by the axial length of the bolt:

$$t = \frac{2L}{c} = 12{\cdot}21\,\mu\text{s}, \tag{5}$$

where $L$ is the total length of the bolt including the bolt head thickness (35·983 mm from Table 1) and $c$ is the wave speed from equation (4). The time span $\Delta t$ of the cycloidal portions of the prescribed motion curves was then selected to be 40 μs so that it was more than 3 times the time value calculated in equation (5). Additionally, the transition portions of the velocity curve were selected to be cycloidal to assure that the acceleration would be continuous and to minimize the magnitude of the acceleration. This curve selection also assured continuous jerk (first derivative of acceleration).

While the selection of the shape of the prescribed velocity reduced the undesirable dynamic effects, another feature of the mesh and the contact algorithm in PRONTO3D [4] tended to reintroduce these effects. Due to the precision of the pre-processing programs a slight overlap existed at some locations of the interface between the thread forms. This led to an initial pushback of the penetrating nodes, which manifested as an initial spike in the kinetic energy (see Figure 5). This acted like an impulse load on the system, introducing high-frequency stress waves that produced undesirable results during the rest of the dynamic simulations.

To remove these dynamic effects two preliminary stages were simulated before the prescribed velocities described above were applied. During the first stage, which lasted 60 μs, node set 1 was held fixed in the axial direction by setting the prescribed velocity to zero and a mass proportional viscous damping was introduced. A proportionality constant of 1·14e6 $\text{s}^{-1}$ was selected to provide the maximum reduction in net kinetic energy for the entire system over the selected simulation time. It can be seen in Figure 5 that the kinetic

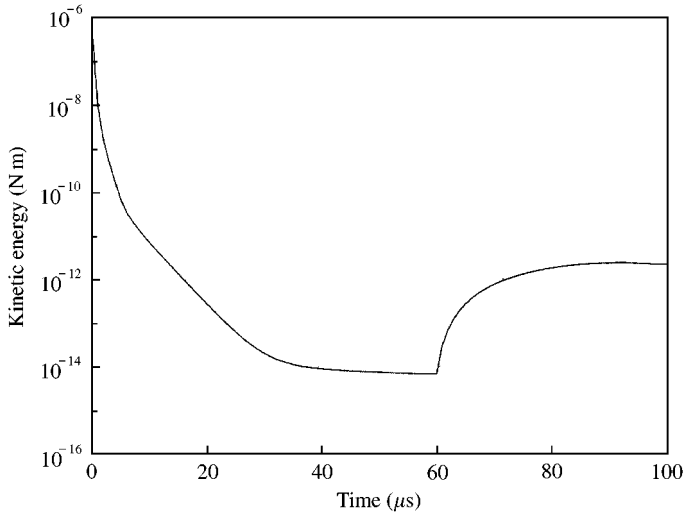


Figure 5. Kinetic energy for the preliminary stages of the dynamic simulations.

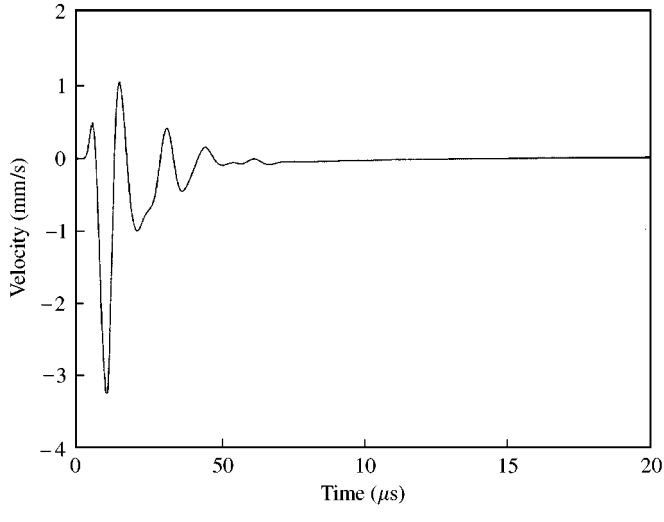


Figure 6. Velocity of node 6 during damped preliminary stage.

energy was reduced by eight orders of magnitude during this simulation stage. During the second stage, which ran from 60 to100 μs in Figure 5, node set 1 continued to be held fixed in the axial direction and the mass proportional viscous damping constant was set to zero. Over this time the kinetic energy increased by more than two orders of magnitude from the minimum but was still more than five orders of magnitude smaller than the original kinetic energy spike.

The velocity of node 6 is plotted in Figure 6 for the first 20 μs of the damped preliminary stage to further illustrate the effects of the initial impulse load due to the pushback and the mitigation of these effects by the mass proportional damping. Node 6 is located on the centerline of the bolt shank on the transverse line that is just above the engagement between the external and internal thread forms (see Figure 3). This node did not begin to move until the seventh time step of the simulation (approximately 0·040 μs) and it then exhibited

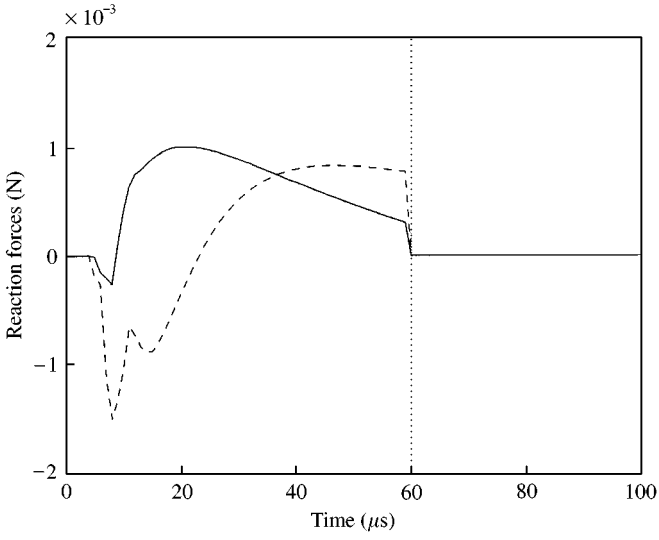


Figure 7. Net reaction forces on node set 1 during the preliminary stages: ——, transverse $x$; – – – – –, transverse $y$.

a positive velocity (i.e., in the opposite direction of the pushback of the external threads). This produced an oscillation that was essentially damped out by 7·50 μs (about 1300 time steps, where the kinetic energy of the system had been reduced by over four orders of magnitude). While the velocity of node 6 did not noticeably oscillate after 7·50 μs, it was also not equal to zero. Indeed, it was approximately equal to $-0{\cdot}055$ mm/s, By the end of the damped preliminary state (60 μs) the axial velocity was reduced to $+7{\cdot}007$ nm/s and the axial displacement was $-2{\cdot}257$ nm.

To assure that the mass proportional damping was not introducing a fictitious solution, a second preliminary stage without damping was run. A fictitious solution was suspected because the transverse components of force on node set 1 were not equal to zero (see Figure 7). The removal of the damping allowed these force components to return to zero immediately, while also allowing the oscillations to reappear. However, the amplitude of the velocity of node 6 was still four orders of magnitude smaller than the maximum amplitude due to the initial shock. During this undamped stage the axial displacement of node 6 was reduced to $-2{\cdot}253$ nm.

At the end of the preliminary stages a small axial force existed in the bolt (see Table 4). It should be noted that the quasistatic simulation was not subject to the impulse-induced oscillations exhibited in the dynamic simulations, and so no preliminary stages were needed.

To qualitatively assess the effect of the preliminary unloaded stages on the results of the subsequent loaded phase two versions of the Case 2 simulation, with and without the preliminary stages, were run. Figure 8 shows the kinetic energy values from these two simulations. As can be seen from this plot, the kinetic energy appears to have smaller fluctuations in the constant velocity regions (where the kinetic energy is maximized) of the simulation run with the preliminary stages used to damp out initial fluctuations due to the pushback. Additionally, the initial kinetic energy spike is seen to be only one order of magnitude smaller than the maximum kinetic energy due to loading. This reduction of the fluctuations in the constant velocity regions of the loading is important, as data from these regions are used to determine the axial stiffness values, as discussed in the next section of this paper.

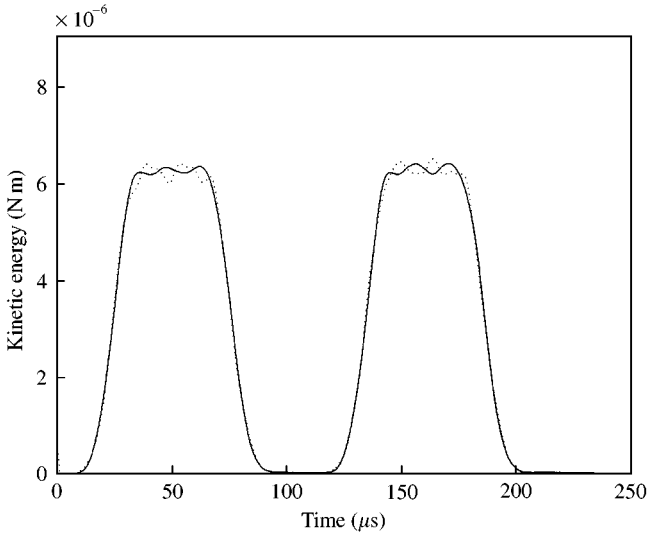


Figure 8. Kinetic energy values for Case 2 simulations: ——, with preliminary stages; ……, without preliminary stages.

TABLE 3

*Axial displacement values*

| Node number | Initial displacement (nm) | Final displacement | | | |
|---|---|---|---|---|---|
| | | Case 1(a) (μm) | Case 1(b) (μm) | Case 2 (nm) | Quasistatic (μm) |
| 1 | 0·0000 | 65·024 | 8·128 | 0·0000 | 8·103 |
| 2 | − 0·402 | 55·928 | 6·988 | − 1·796 | 6·974 |
| 6 | − 2·253 | 14·221 | 1·775 | − 8·820 | 1·732 |
| 9 | − 2·896 | 2·653 | 0·331 | − 10·752 | 0·322 |

## 4. DETERMINATION OF AXIAL STIFFNESS

For the results presented below, the unloaded preliminary stages are not included. Therefore, the initial time (0 μs) corresponds to the end of the second (undamped) preliminary stage and to the initial time of the displacements shown in Figure 4.

Figure 9 shows the axial displacements of four nodes as determined by the Case 1(a) simulation. Node 1 is a member of node set 1, so its displacement is equivalent to the prescribed displacement of Figure 4. Node 2 is the node on the bolt centerline at the top of the bolt head. Nodes 6 and 9 also lie on the bolt centerline and are located just above the top of the thread engagement and at the end of the bolt body, respectively, as shown in Figure 3. It should be noted that there are small initial displacements of nodes 2, 6, and 9 due to the thread pushback of the preliminary stages. The values of these initial displacements are listed in Table 3 along with the values of the final displacements for the three dynamic and the quasistatic loading cases. The final displacements from Case 1(a) are all 8 times as large as the final displacements from Case 1(b), as would be expected due to the ratio of velocity scale factors. The final displacements from the quasistatic analysis are not exactly

TABLE 4

*Axial load values*

| Initial load (kN) | Final load (kN) | | | |
|---|---|---|---|---|
| | Case 1(a) | Case 1(b) | Case 2 | Quasistatic |
| 0·0005 | 10·8770 | 1·3622 | 0·0021 | 1·3845 |

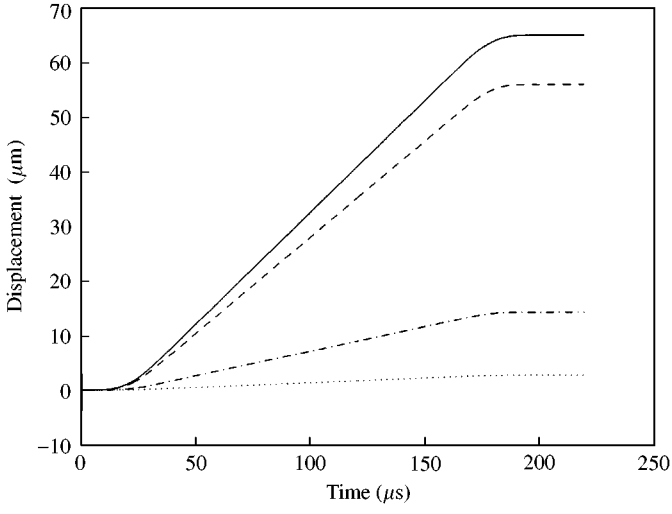


Figure 9. Axial displacements from Case 1(a): ——, Node 1; – – – – –, Node 2; –·– – ·–, Node 6; ····, Node 9.

proportional to the final values from dynamic Case 1(b), though the largest variation is less than 3%, which is well within acceptable bounds. Additionally, the final displacements for Case 2 are not equal to the initial displacements, except for node 1 which is prescribed. This means that while the loading condition is fully reversed the FEM solution is not.

The axial load is determined differently for the dynamic and quasistatic simulations due to the way in which the two FEM codes (PRONTO3D and JAS3D, respectively) handle load calculations. For the dynamic simulations, the axial load is found by summing the $z$-component of the nodal reaction forces for all of the nodes in the bolt head mesh. For the quasistatic simulations, the axial load is equal to the net force in the $z$-direction on the entire model. Time histories of the axial load for all of the simulations are shown in Figure 10. Initial and final values for the axial load are summarized in Table 4. Again, the final load from Case 1(a) is 8 times as large as the final load from Case 1(b), as would be expected. The final load from the quasistatic simulation is larger than the final load from Case 1(b), which is not expected since the final displacement from the quasistatic simulation is smaller that the final displacement from Case 1(b) (see Table 3). Also, the final load from Case 2 is not equal to the initial load for the dynamic cases, which is in keeping with the changes in final displacements as noted above.

With the axial displacements and loads discussed above, the axial stiffness of the bolt can be calculated. The most straightforward method to calculate the axial stiffness $k_{axial}$ would be to divide the axial force $F_{axial}$ by the axial displacement $z$:

$$k_{axial} = F_{axial}/z. \tag{6}$$

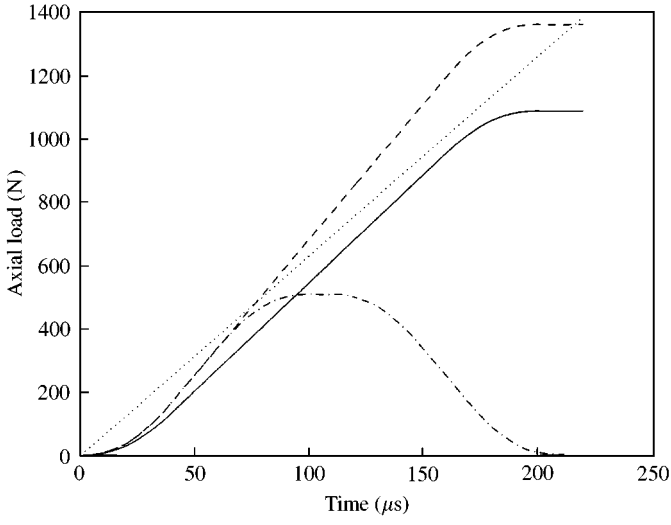


Figure 10. Time histories of the axial load. Note: The values for Case 1(a) have been reduced by a factor of 10: ——, Case 1(a) (/10); – – – – – –, Case 1(b); – · – – · – – · – – · –, Case 2; · · · ·, quasistatic.

TABLE 5

*Regions used for curve fits*

| Dynamic case | Loading (μs) | Unloading |
|---|---|---|
| 1(a) | 36–164 | N/A |
| 1(b) | 36–164 | N/A |
| 2 | 36–64 | 146–174 μs |

This approach would be valid for the quasistatic simulations, where $F_{axial}$ and $z$ are both initially equal to zero and where the axial force is only due to the bolt stretch. In the dynamic simulations, the value determined from equation (6) would be invalid, since neither $F_{axial}$ nor $z$ is initially equal to zero and since the calculated axial force is a resultant of the forces due to bolt stretch and to the acceleration of the bolt head. The non-zero initial values can be addressed by using a least-squares linear curve fit which would lead to an expression of the form

$$F_{axial} = F_o + k_{axial} z, \tag{7}$$

where $F_o$ is an offset value. The effects of acceleration can be minimized by the using the $F_{axial}$ and $z$ data from the regions of the loading curves where the prescribed velocity is nearly constant. The time values that delimit these regions for the three dynamic load cases are listed in Table 5. It should be noted again that the preliminary stages that were used to reduce fluctuations due to the initial pushback at the threads (see Figure 8) are also critical in minimizing dynamic effects during the loading stages.

A final question that arises in the calculation of $k_{axial}$ in equation (7) is which axial displacement $z$ should be used. The first option would be to use the prescribed displacement $z_1$. The error in this approach is illustrated in Figure 9 and Table 3, where it can be seen that the displacement $z_9$ at the opposite (threaded) end of the bolt is not zero. Indeed, the final

values of $z_9$ for dynamic Cases 1(a) and 1(b) and the quasistatic case are all 4% of the final values of $z_1$. To account for this motion of the end of the bolt, the displacement $z$ in equation (7) should be replaced by a relative displacement value $\Delta z$:

$$F_{axial} = F_o + k_{axial}\Delta z. \tag{8}$$

Then $\Delta z$ might be defined as the difference between $z_1$ and $z_9$. Using this approach, with the quasistatic data and assuming that $F_o = 0$, the value of $k_{axial}$ is found to be 177·9 MN/m, while the value determined in reference [1] by matching experimental data was 245·2 MN/m.

A second option would be to use the displacement $z_2$ at the center of the bolt head in place of the prescribed displacement $z_1$. This would be justified, as it would represent the axial stretch of the bolt's centerline. Defining $\Delta z$ as the difference between $z_2$ and $z_9$, the value of $k_{axial}$ is found to be 208·1 MN/m, which is closer to the value determined in reference [1].

A third option reveals itself after closer inspection of the phenomenon being modelled. The value of $k_{axial}$ was used in reference [1] to determine the reduction of axial force due to a rigid body rotation of the bolt body. In this application it appears that $\Delta z$ should be a measure of the stretch of the bolt from the threads to the head. Therefore, $\Delta z$ is defined to be the axial stretch along the centerline from the top of the bolt head to the point in the bolt shank just above the engagement between the external and internal threads (node 6 of Figure 3):

$$\Delta z \equiv z_2 - z_6. \tag{9}$$

Using this definition of $\Delta z$ and a standard least-squares linear curve fit routine, values for $k_{axial}$ and $F_o$ for the four loading cases are determined (see Table 6). From Table 6 it can be seen that the stiffness values are 5·6–7·7% higher than the value used in reference [1], which is well within the tolerance used to determine that value. The variation among the four values from the dynamic simulations is less than 1%, while the quasistatic value is 1·5% larger than the average of the dynamic values, which is well within the precision of the codes. The variation among the values of the offset $F_o$ is larger, though all of the values are small in comparison with the average load values for the respective simulations. The $R^2$ values are all nearly equal to unity, indicating that the linear curves match the data very well. One interesting thing about the offset values is that they do not seem to correlate with the initial load values listed in Table 4.

To check the results obtained from the FEM analyses, the value of the axial stiffness of the bolt could be approximated by considering it to be a simple cylinder [6]:

$$k_{axial} = AE/L, \tag{10}$$

where $A$ is the cross-sectional area,

$$A = \frac{\pi}{4}d^2, \tag{11}$$

$E$ is Young's modulus, $L$ is the length of the cylinder, and $d$ is the diameter of the cylinder.

Using the values from Tables 1 and 2, assuming a constant diameter for the entire bolt and a length equal to the total length of the bolt (from node 2 to 9), leads to $k_{axial} = 182{\cdot}0$ MN/m. This value is considerably smaller than the equivalent value from the FEM analyses reported above (208·1 MN/m). If the value of $L$ in equation (10) is changed from the total length of the bolt to the axial distance between nodes 2 and 6 (25·8233 mm), then $k_{axial} = 253{\cdot}6$ MN/m. This value lies between the value used in reference [1] to match

TABLE 6

*Least-squares curve fit values*

| Load case | $k_{axial}$ (MN/m) | $F_o$ (N) | $R^2$ | Average load (N) |
|---|---|---|---|---|
| 1(a) | 260·9 | 4·066 | 0·999999 | 5446· |
| 1(b) | 261·3 | 0·072 | 0·999997 | 681·5 |
| 2 (loading) | 259·6 | 0·140 | 0·999966 | 254·9 |
| 2 (unloading) | 259·1 | 0·618 | 0·999913 | 254·4 |
| Quasistatic | 264·1 | − 0·080 | 1·000000 | 692·2 |
| 1(a) (revised) | 259·1 | 5·298 | 1·000000 | 5707· |
| Quasistatic (refined) | 274·4 | − 0·105 | 0·999999 | 743·6 |

the experimental data (245·2 MN/m) and those determined from the FEM model as listed in Table 6.

These comparisons show that the hand calculations are sometimes accurate, and sometimes very inaccurate. Additionally, there exists a question as to how to model the bolt stiffness using the method of equation (10). In reference [7] several alternatives were proposed, and the nominal value reported in reference [1] was based on modelling the bolt as a pair of cylinders with different diameters acting in series, to account for the reduced diameter of the threaded section. This model led to a value of 161·8 MN/m, which is almost 20% lower than the value predicted by the FEM results using the equivalent relative deformation. While a reasonable value for the axial stiffness can be calculated using equation (10), the reader is reminded that the values used in this calculation were not obvious until after the FEM results had been examined.

## 5. ADDITIONAL RESULTS AND DISCUSSION

The axial stiffness results that were presented in the previous section of this paper appeared to be quite satisfactory. The axial load versus stretch curves were essentially linear and nearly reversible, indicating linear elastic behavior as expected. Additional results are presented in this section to confirm the appropriateness of the FEM results, and to highlight differences between the PRONTO3D dynamic results and the JAS3D quasistatic results.

Figure 11 shows an elevated view of the deformed mesh at the final time for the Case 1(a) dynamic simulation. The deformations have been multiplied by 500 to improve the visualization. This deformation pattern seems to be reasonable for the loading case. The only area of the model where the deformation pattern may not meet expectation is the bolt head. For comparison, Case 1(a) was revised by setting the radial velocity of node set 1 to zero. Combined with the loading condition for Case 1(a), this new boundary condition forced the outside of the bolt head to retain its original shape with the center of the hexagon fixed at the bolt axis (in the $x$, $y$ planes). Therefore, the only free displacement of node set 1 would be a rotation about the bolt axis. The magnified deformation pattern for this revised simulation is shown in Figure 12. Comparing Figure 12 to Figure 11, the only obvious differences occur at the bolt head.

Zoomed cross-sectional views of this area for the two simulations are shown in Figure 13. Here it can be seen that the major affect of the revised boundary condition was the reduction of the deformation of the center of the bolt head, which would lead to a larger

Figure 11. Deformed mesh at the final time for Case 1(a) (deformation magnified by a factor of 500).

calculated value for the axial stretch. This increase in stretch was determined to be 5·5% over the constant velocity region of the loading case used to determine the value of $k_{axial}$. However, the average axial load over this region increased by 4.8%, so that the calculated axial stiffness value decreased by 0·7% (see Table 6). Since it was the latter value which was of primary interest in this study, this comparison shows that the original boundary conditions, which left node set 1 free in all but the axial direction, were appropriate despite the unexpected deformation of the bolt head.

The kinetic energy functions for Case 1(a) and its revision are presented in Figure 14. This plot shows that restraining the outside of the bolt head to only rotation about the bolt axis increased the net kinetic energy of the system, and reduced the oscillations of this function during the constant velocity portion of the loading cycle.

A zoomed cross-sectional view of the first thread engagement at the final time of the original Case 1(a) simulation (equivalent to Figure 11) is shown in Figure 15. This figure includes an undeformed view and a deformed view magnified by 100 of the same zoom window, and it can be seen that the fixed contact between the bolt body and the external threads and between the plate and the internal threads was enforced. The contact between the two thread forms was also enforced, even as the external threads bent and rotated. The top of the plate was deformed slightly in the same direction as the loading, as would be

Figure 12. Deformed mesh at the final time for the revised Case 1(a) (deformation magnified by a factor of 500).

expected, and the deformation patterns in the thread forms were also consistent with expectations.

A final comparison between the original and revised Case 1(a) results is shown in Figures 16 and 17. These plots show the deformations of node lines from four axial locations in the bolt body. The first of these locations was at the top of the bolt head, while the three other locations were in the threaded portion. The axial distance between the first and second locations was 25·823 mm, while the distances between the second and third and third and fourth locations were both 5·080 mm. The larger distance between the first and second locations was the reason why the axial deformations ($\Delta z$) increased more dramatically over this span. In general, the axial deformations were nearly equal across a transverse line, though there was a slight dip at the center of the node 2 location (corresponding to the magnified deformations seen in Figures 11 and 12) and a slight rise in the centers of the other three locations.

The in-plane deformations ($\Delta y$) show how transverse cross-sections rotated during loading. The section at the threaded end of the bolt (node 9) rotated about the bolt axis. Moving up the bolt axis, the cross-sections not only rotated but also translated in the positive $y$-direction, with the amount of translation increasing with increasing axial position. This trend continued to the top of the bolt head in the simulation with the original

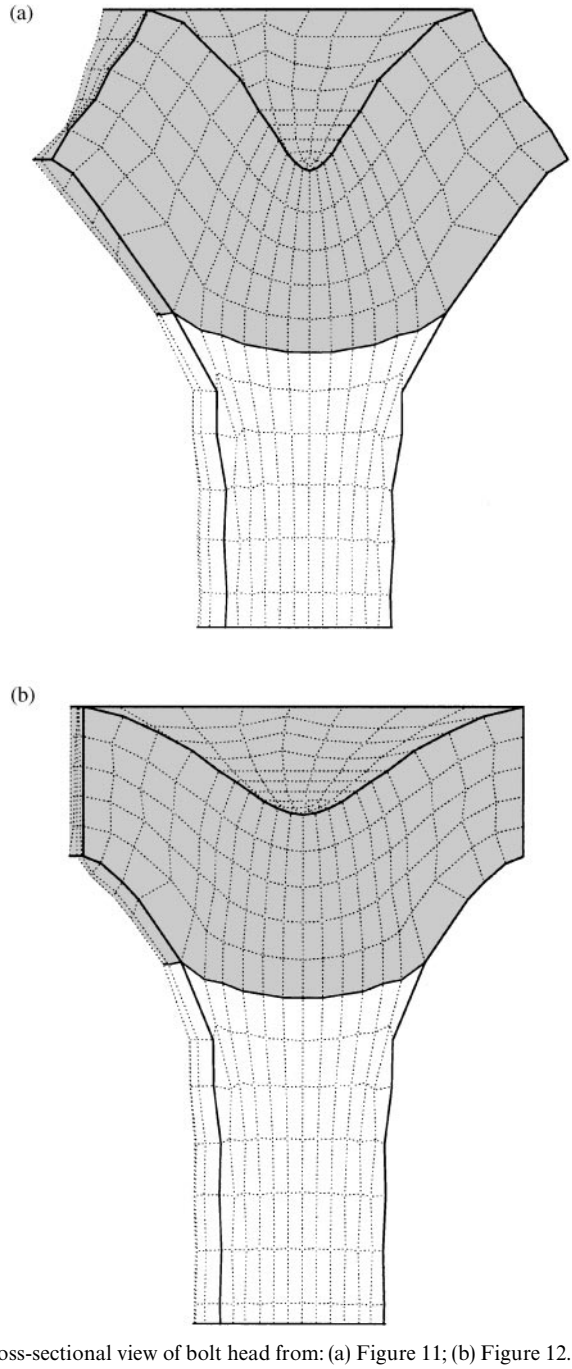


Figure 13. Zoomed cross-sectional view of bolt head from: (a) Figure 11; (b) Figure 12. Deformations magnified by a factor of 500.

boundary conditions (Figure 16). In the simulation with the revised boundary conditions, the top of the bolt head only rotated, as expected. The additional boundary condition also reduced the amount of translation experienced by the intermediate cross-sections (Figure 17). It should be noted that the cross-sections also contracted, as would be expected

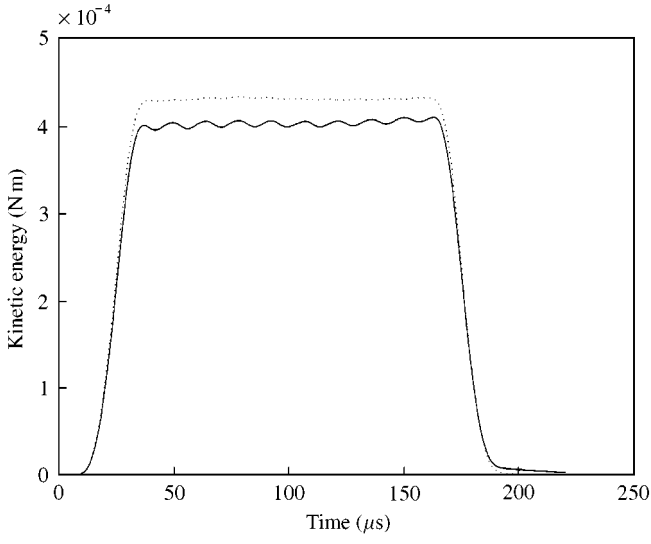


Figure 14. Kinetic energy for Case 1(a) (free) and its revision (fixed): ——, free; ····, fixed.

from the Poisson ratio effects, though this change in the length of the radial lines is imperceptible in Figures 16 and 17 due to the scaling of the $x$-axis.

Figure 18 shows zoomed cross-sections of the system for two different dynamic load cases and the quasistatic load case for times when the calculated axial loads were approximately 1290 N. The actual loads for these plots were 1291·6 N (Case 1(a)), 1288·5 N (Case 1(b)), and 1290·1 N-(quasistatic case). The shaded contours correspond to different levels of the von Mises stress. The plots from Cases 1(a) and 1(b) are nearly identical, while the plot for the quasistatic case is quite similar. In all cases the stress is nearly zero at the outside of the bolt head, at the center of the bolt head where it attaches to the shaft, at the threaded end of the bolt, and in the plate. The latter two locations are as expected, while the former two may not have been expected but are consistent with the displacement pattern of Figure 13. The stress is largest at the base of the first thread forms that are engaged, as would be expected (note that scale goes from 0 to 84 MPa). The stress then decreases in both directions along the bolt axis, with the drop off being faster toward the threaded end than toward the bolt head. Assuming perfect axial stress in the unthreaded portion of the bolt shaft, the nominal stress level would be predicted to be 40·679 MPa. The loading is not perfectly axial, but the nominal stress in the center of the unthreaded portion of the shaft is found to be approximately 41·437 MPa for the dynamic cases shown in Figure 18 and 41·162 MPa for the quasistatic case, which are only 1·9% and 1·2% increases, respectively, over the simple "force divided by area" value.

The corresponding plot of von Mises stress distribution from the revised version of the Case 1(a) loading conditions is included in Figure 19. Here the axial load was calculated to be 1287·6 N These results are very similar to those for the original Case 1(a) loading conditions included in Figure 18(a), with noticeable differences in the patterns being restricted to the bolt head and the unthreaded portion of the shank. The most significant changes were in the bolt head, where the stress at the top surface was reduced and where the area of reduced stress in the center of the head was raised and reshaped. Additionally, the nominal stress in the unthreaded portion of the shank was reduced to approximately 41·162 N.

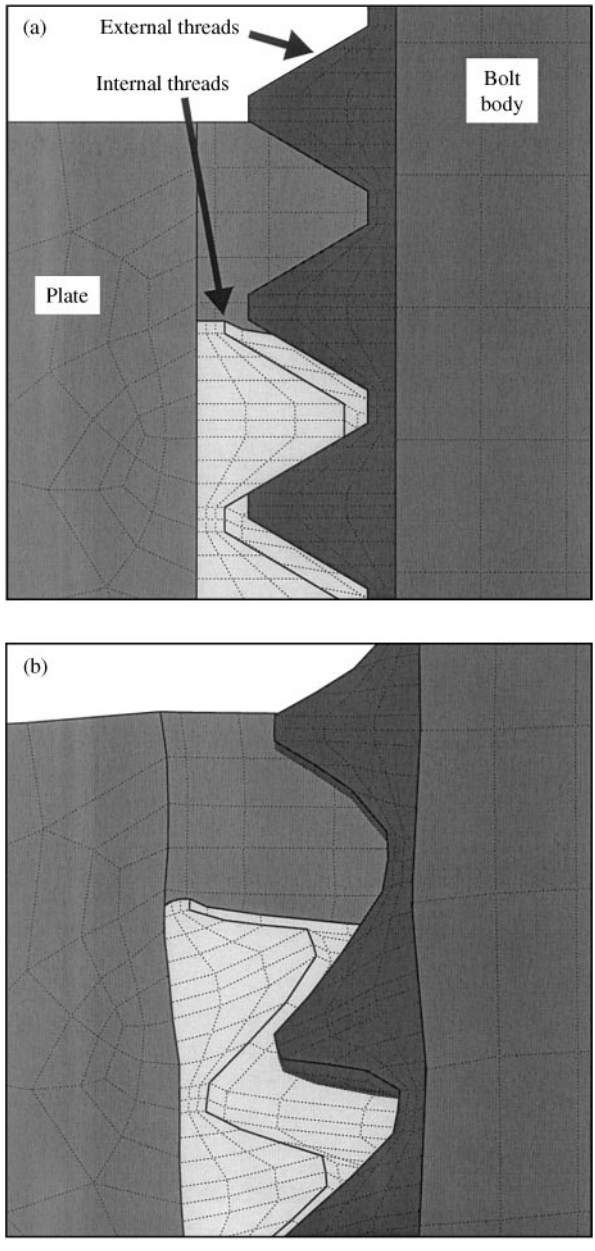


Figure 15. Zoomed cross-sectional view of threads from Figure 11: (a) undeformed mesh; (b) deformed mesh magnified by a factor of 100.

A refined mesh was also developed in reference [3]. A version of this mesh was also analyzed under axial loading using JAS3D and the results were compared with the coarse mesh results presented above. The quasistatic analysis was chosen for this comparison because it required significantly less computational time than the dynamic analyses. The coarse mesh quasistatic analysis (JAS3D) required 3·04 CPU h on a Sun UltraSPARC-II workstation (single processor with 296 MHz clock speed), while a complete dynamic

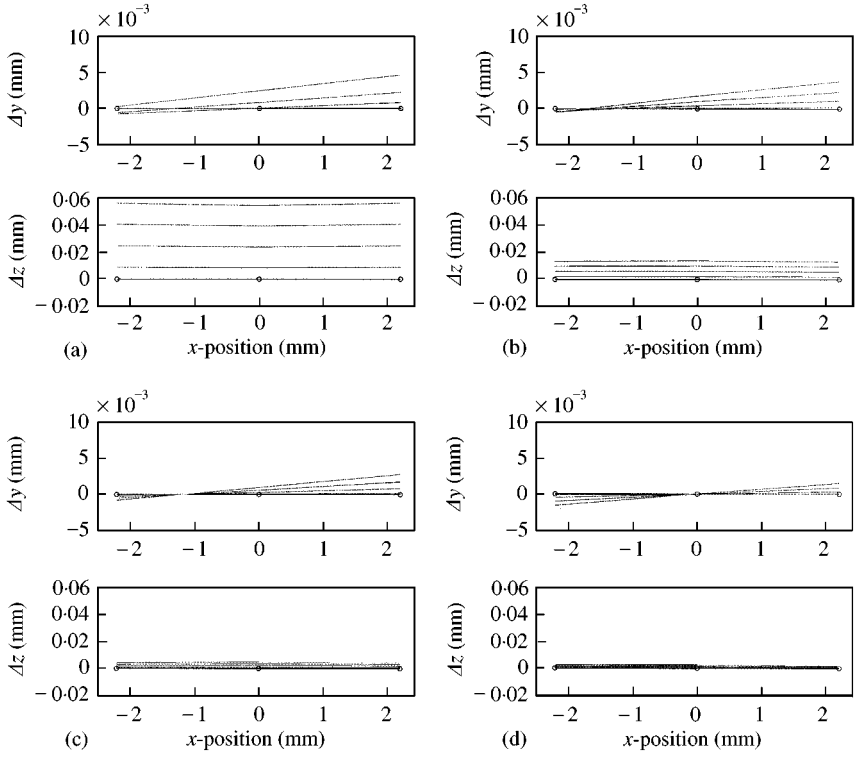


Figure 16. Displacement of node lines that lie along the $x$-axis at different vertical positions for Case 1(a): (a) top of bolt head (node 2); (b) just above thread engagement (node 6); (c) mid-point between nodes 6 and 9; (d) free end of bolt (node 9). Note: node numbers correspond to Figure 3. Circles (o) mark the undeformed lines while crosses (x) mark the deformed lines at the final time.

analysis (PRONTO3D) of the same mesh (i.e., including the two preliminary stages and the loading stage) took 57·66 CPU h on the same computer. The refined mesh quasistatic analysis (JAS3D) required 32·60 CPU hours, or a factor of 10·72 times longer than the coarse mesh. Extrapolating this time increase to the dynamic analysis leads to an estimate of over 618 CPU h or nearly 26 CPU days.

As reported in reference [3] the major differences between the coarse and refined meshes involved the refinement of the thread meshes, including the rounding of the thread roots and crests, and the addition of a chamfer where the bolt head connected to the unthreaded shank. Otherwise, every attempt was made to assure that the two models had the same dimensions. However, the differences in the meshing approaches did lead to slight differences in nodal locations. In particular, the axial distance between nodes 2 (top of bolt head) and 6 (just above the first thread engagement) increased from 25·400 mm in the coarse mesh to 25·823 mm in the refined mesh. This 1·67% increase accounted for just under half of the 3·89% increase in the calculated value of the axial stiffness, as reported in Table 6. Other differences could be attributed to the fact that the external (bolt) threads were shifted by approximately half the thread pitch, as can be seen by comparing Figures 3 and 20. Additionally, there could be as much as 1·00% difference between the results due solely to the selected convergence tolerance for the iterative solution scheme in JAS3D. The von Mises stress distributions shown in Figures 18(c) and 21 (where the axial load was calculated to be 1284·7 N) are seen to be quite similar. The major differences lie in the bolt

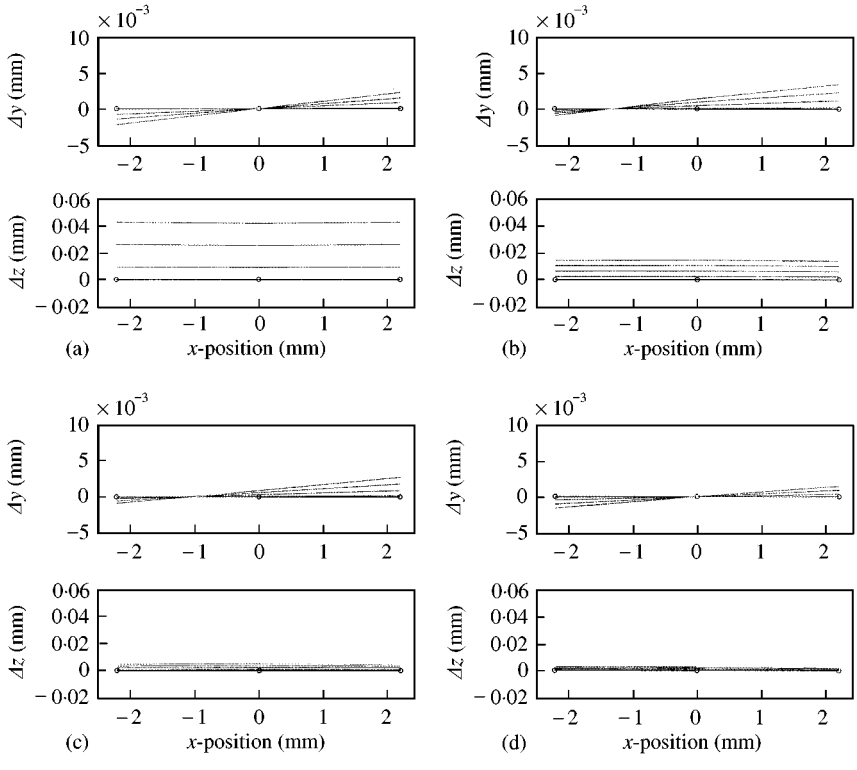


Figure 17. Displacement of node lines that lie along the $x$-axis at different vertical positions for the revised version of Case 1(a): (a) top of bolt head (node 2); (b) just above thread engagement (node 6); (c) mid-point between Nodes 6 and 9; (d) free end of bolt (node 9). Note: node numbers correspond to Figure 3. Circles (o) mark the undeformed lines while crosses (x) mark the deformed lines at the final time.

head area, where the refined mesh had a lower maximum value along the top edge, increased stress at the outer corners, an increased area of reduced stress in the middle that was shifted up, and significant stress intensification at the chamfers. The area of increased stress that appeared in the coarse mesh results, about one-third of the way down in the unthreaded portion of the shank, is missing from the refined mesh results. Stress intensification at the roots of the external threads was not as severe in the refined mesh results, though this may be an artifact of the reduced size of the elements in this region. Additionally, the nominal stress in the unthreaded portion of the shank was reduced to approximately 40·610 MPa.

## 6. COMPUTATIONAL CONSIDERATIONS

The FEM analyses presented in this paper are computationally intensive and, until very recently, would have been restricted to the very fastest super computers. The results presented in this paper were all generated on a mid-range UNIX workstation, using a single processor (Sun UltraSPARC-II with a 296 MHz clock speed). This machine was upgraded from its standard configuration by adding RAM (to 640 Mbytes) and hard disk space (to 12 Gbytes). Even with these upgrades, only two simulations could be run simultaneously, results needed to be deleted or reduced in size on a regular basis to assure adequate hard disk space for additional analyses, and complete simulations might take days to be processed.

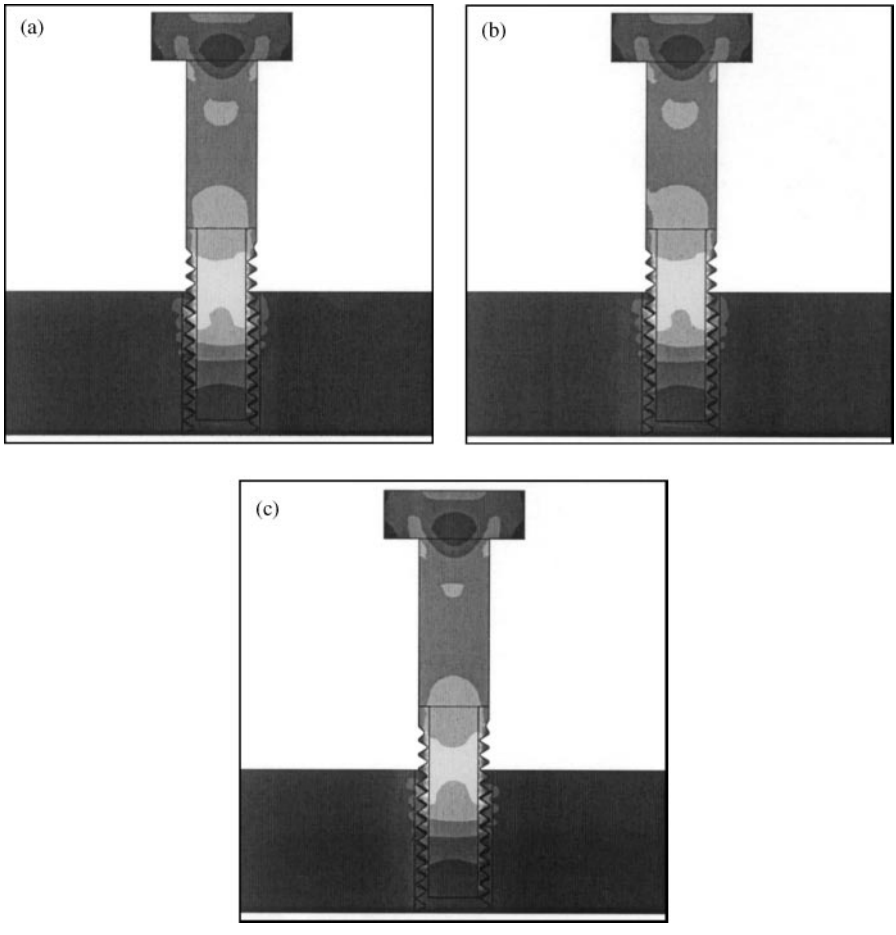


Figure 18. Von Mises stress when axial load is approximately 1290 N (cross-sectional view): (a) Case 1(a); (b) Case 1(b); and (c) quasistatic case.

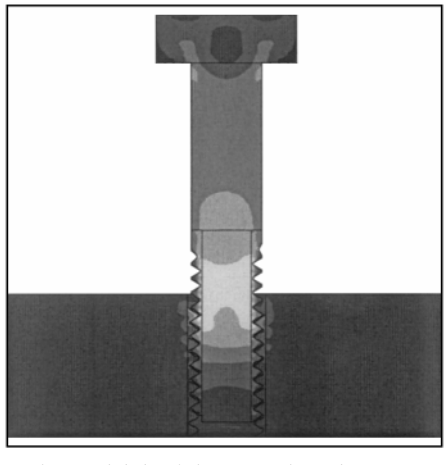

Figure 19. Von Mises stress when axial load is approximately 1290 N for revised Case 1(a) loading (cross-sectional view).

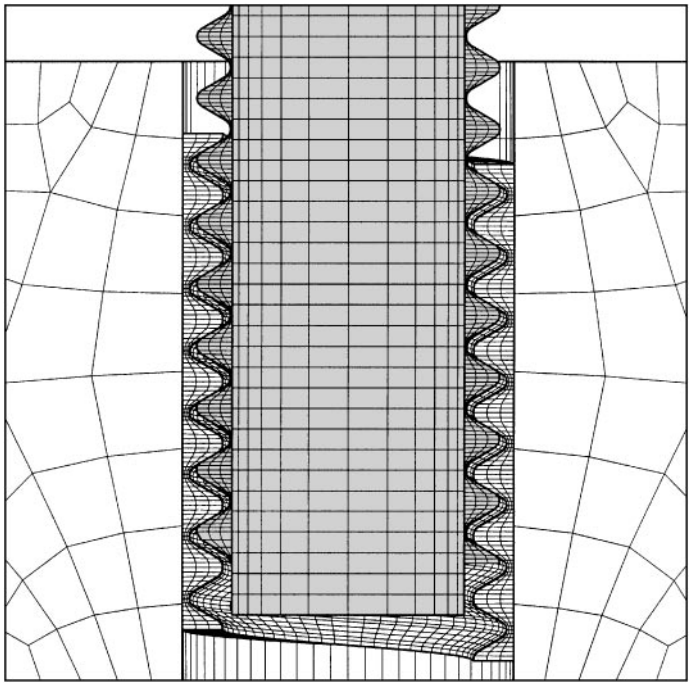

Figure 20. Cross-sectional view of the mesh zoomed at the threads for the refined mesh.

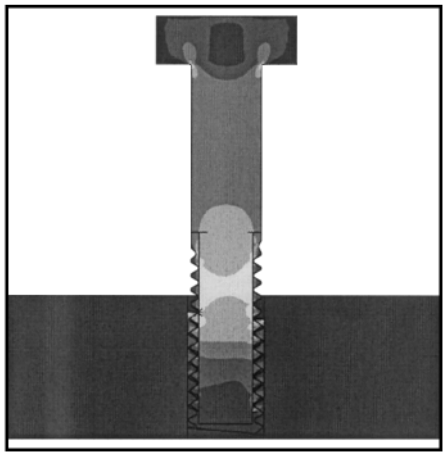

Figure 21. Von Mises stress when axial load is approximately 1290 N for refined mesh and quasistatic loading (cross-sectional view).

As reported above, a complete dynamic analysis (PRONTO3D) of the coarse mesh (i.e., including the two preliminary stages and the loading stage) required 57·66 CPU h (2·4 CPU days), 11 Mbytes of RAM, and 1·50 Gbytes of hard disk space. Since the preliminary stages did not need to be repeated, it was possible to reduce the time and hard disk space required for subsequent analyses. A typical dynamic analysis including only the loading stage required 40·79 CPU h (1·7 CPU days) and 0·98 GBytes of hard disk space. The equivalent quasistatic analysis (JAS3D) of the same mesh required 3·04 CPU h, 13 Mbytes of RAM, and 0·19 Gbytes of hard disk space. The refined mesh quasistatic analysis

required 32·60 CPU h (1·4 CPU days), 39 Mbytes of RAM, and 0·60 GBytes of hard disk space.

## 7. CONCLUSIONS

Six three-dimensional finite element analyses of a model of a threaded connection involving a single bolt threaded into a plate have been presented. Five of these analyses employed the same finite element mesh (coarse mesh) while the sixth analysis employed a refined version of this mesh. Four of the coarse mesh analyses utilized a dynamic solution program called PRONTO3D, while the fifth coarse mesh analysis and the refined mesh analysis utilized a quasistatic solution program called JAS3D. In all of these analyses the bottom of the plate was held fixed in all directions while kinematic constraints were used to pull the bolt in its axial direction.

The results from these FEM outputs were then analyzed to determine values for the axial stiffness of the bolt. These values were based on the axial stretch measured between two nodes, one at the top of the bolt head and a second in the bolt body just above the first thread engagement, which were located on the bolt axis, and an equivalent axial force. The results from all six analyses were in good agreement, and these results agreed with the value presented by Zadoks and Yu in their prediction of the self-loosening of a threaded connection [1]. The FEM results were compared with hand calculations, and it was found that good agreement could be achieved using dimensions that were selected based on the FEM results. Additional FEM results were presented to further confirm the appropriateness of the solutions.

There are two significant conclusions that can be drawn from the work presented here. First, it has been shown that the complex three-dimensional behavior of a threaded connection, including contact between helical threads, can be accurately modelled using the PRONTO3D dynamic analysis finite element method computer software [4]. This lays the groundwork for analyses with more complex loading conditions, such as the tightening of a bolt to create a preload and the transverse vibration of the entire bolted connection with bolt preload. Second, the results of these analyses confirm the value of axial stiffness that had been derived empirically in reference [1], and provide clear insight into why this value is correct.

## ACKNOWLEDGMENTS

This work was supported by the Sandia National Laboratories through Contract AO-3571 with The University of Texas at El Paso. The authors are especially indebted to Martin Heinstein for his advice in developing the mesh of the threads and the refined bolt mesh used in this work, and to Stephen Attaway for sponsoring this effort. The authors would also like to thank Mark Blanford, Kevin Brown, Sam Key, and Gregory Sjaardema for their assistance.

## REFERENCES

1. R. I. ZADOKS and X. YU 1997 *Journal of Sound and Vibration* **208**, 189–209. An investigation of the self-loosening behavior of bolts under transverse vibration.
2. D. P. HESS 1995 in *Vibration of Nonlinear, Random, and Time-varying Systems, American Society of Mechanical Engineers* **DE-84**, 1165–1170. Vibration-induced loosening and tightening of threaded fasteners.
3. R. I. ZADOKS and D. P. R. KOKATAM 1999 *Computer Modeling and Simulation in Engineering* **4**, 274–281. Three-dimensional finite element model of a threaded connection.

4. S. W. ATTAWAY, F. J. MELLOW, M. W. HEINSTEIN, J. W. SWEGLE, R. I. ZADOKS and J. A. RATNER 1998 *Users' Instructions for PRONTO3D: A Transient Dynamic Code for Nonlinear Structural Analysis. SAND 98-1361*, Albuquerque, NM: Sandia National Laboratories.
5. M. L. BLANFORD 1996 *JAS3D*: *A Multi-Strategy Iterative Code for Solid Mechanics Analysis, Release* 1.4 (Internal report), Albuquerque, NM: Sandia National Laboratories.
6. J. E. SHIGLEY and L. D. MITCHELL 1983 *Mechanical Engineering Design*. New York: McGraw-Hill Book Company. Fourth edition.
7. X. YU 1994 *Ph.D. Dissertation*, *The University of New Mexico, Albuquerque.* Investigations of self-loosening of bolts under vibration.